

Theoretical Study of the Cavitation Mechanism of the Twinkling Artefact in the Ultrasound Imaging of Kidney Stones

A. I. Polyanskiy^{a, *} and O. A. Sapozhnikov^{a, **}

^aMoscow State University, Moscow, 119991 Russia

*e-mail: ai.polyanskiy@physics.msu.ru

**e-mail: oleg@acs366.phys.msu.ru

Abstract—A numerical model is constructed that allows signals of diagnostic ultrasonic pulses scattered on stones and bubbles to be obtained. The model is based on numerical simulation of the equations of elasticity, which describe the propagation of a small-amplitude perturbation in a solid medium, and on the Nolting–Nepiras equation, which describes the dynamics of a gas bubble. The Doppler processing of the obtained signals is performed with the subsequent construction of an ultrasound image. Results show that the cavitation of gas bubbles produces the twinkling artefact.

DOI: 10.3103/S1062873818050258

INTRODUCTION

Ultrasound (US) studies play an important role in modern medicine [1]. An example is the diagnostics of urolithiasis, the formation of kidney stones. One problem is that some stones are difficult to detect by standard modes. Detection can be improved using the so-called twinkling artefact. These are twinkling regions (nonstationary multicolor mosaic structures) that sometimes occur during ultrasonography at the border of an observed image of a kidney stone in the Doppler mode [2, 3].

The mechanisms that underlie the twinkling artefact during ultrasonography are still a subject of debate. The artefact could be caused either by the acoustic treatment, the reflection of an ultrasound pulse from a stone, or by hardware effects associated with processing the signals collected by the detectors. Studies of the twinkling artefact with different types of stones show that the effect depends on the morphological and biochemical composition of the stones and varies from measurement to measurement. The intensity of the artefact also depends on the pulse repetition frequency in an ensemble in the Color Doppler mode. It is still not entirely clear what causes the twinkling artefact.

A possible reason for the occurrence of a flickering picture in the Doppler image of a stone is the sporadic activity of submicron bubbles located in crevices on the rough surface of the stone. The experiment performed in [4] confirmed it is not a hardware–software effect, but the acoustic treatment that causes a twinkling artefact. One of the most important results from the experiment in [4] was the complete suppression of the Doppler signal when the static pressure was raised

to 8.5 MPa, and the restoration of the signal when the pressure returned to its initial value. Since other possible reasons for the artefact (e.g., the force of radiation, reflection from the rough surface, or intrinsic fluctuations from the phase jitter [5]) are not sensitive to an increase in static pressure, the above observation strongly suggests it is bubbles that are the source of the Doppler shift.

The aim of this work was a numerical analysis of the cavitation mechanism, specifically to construct a model that would allow us to test the hypothesis of the contribution from the activity of bubbles to the Doppler signal.

MODEL

The simulation process can be divided into several consecutive stages: (1) calculating the acoustic field during the propagation of ultrasound pulses in an inhomogeneous medium, which in the considered problem is a kidney with a solid inclusion in the form of a kidney stone; (2) simulating the dynamics of bubbles upon the specified acoustic treatment calculated at the first stage; (3) calculating additional scattering signals that occur due to the emission of acoustic waves by oscillating bubbles; (4) constructing ultrasound images in the Doppler mode.

At the above stages of simulation, we used different simplifications that were based on physical features of the considered processes. The bubbles were assumed to be negligibly small when compared to the size of the stone, and to the wavelength of the probing signal. This allowed us to analyze the scattering by the kidney stone, first with no bubbles and then with bubble pul-

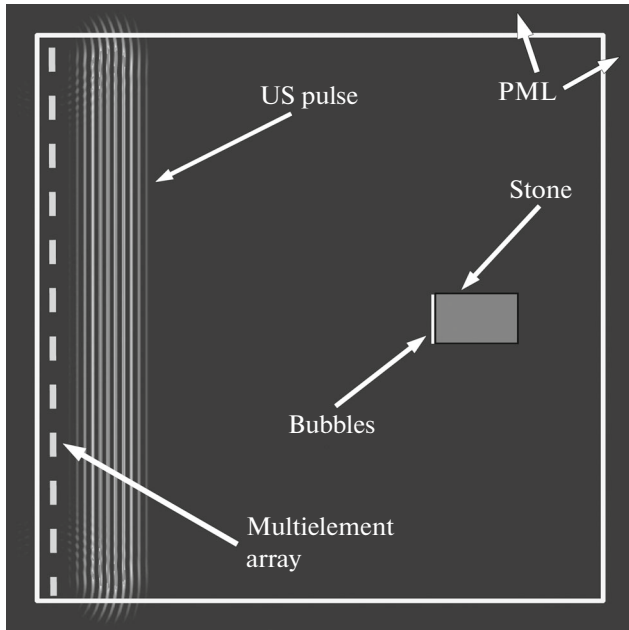


Fig. 1. Experimental scheme in a two-dimensional geometry.

sations in the calculated (specified) acoustic field. Another simplification was associated with the special geometry of the problem: the probing acoustic field and kidney stones were assumed to be axially symmetric. This allowed us to simulate elastic waves in the stone and the surrounding fluid using a two-dimensional model. One more simplification was assuming that the bubbles were spherical in order to describe the dynamics using the Nolting–Nepiras model [6].

Simulating the Propagation of an Ultrasound Pulse

Ultrasound diagnostics is based on the pulse echo imaging of inhomogeneities in human tissue. Ultrasound signals of different durations and frequencies can be used, depending on the chosen mode of study. Conventional signals are microsecond pulses in the megahertz frequency range.

Constructing images in the Doppler mode is based on irradiating a studied medium with a periodic train of pulses (an ensemble) and receiving signals scattered by inhomogeneities. Theoretical investigations of the propagation of ultrasound pulses in soft biological tissues conventionally use an approach that considers the acoustic properties of the tissue to be similar to those of classical fluids, the dynamics of which is described by the equations of fluid dynamics. But kidney stones are solid bodies, so their shear elasticity must be taken into account. The separate description of the stones and soft tissues results in the need to introduce boundary conditions. However, we may assume the entire area of interest is one inhomogeneous medium [7]. Inhomogeneity means a change in the elastic modulus and density upon moving from one region of the

medium to another. In this approach, the boundary conditions at the internal interfaces are met automatically. This simplification also allows us to use the same equations for two media.

The amplitudes of ultrasound signals in our simulation were selected to be close to the values used in ultrasound diagnostics (no more than 1 MPa). The low amplitudes allows us to consider the problem using a linear approximation, and to use equations of elasticity, which include equation of motion and Hooke's law [8]:

$$\rho \frac{\partial v_i}{\partial t} = \frac{\partial \sigma_{ij}}{\partial x_j} + f_i, \quad (1)$$

$$\frac{\partial \sigma_{ij}}{\partial t} = \lambda \frac{\partial v_l}{\partial x_l} \delta_{ij} + \mu \left(\frac{\partial v_i}{\partial x_j} + \frac{\partial v_j}{\partial x_i} \right), \quad (2)$$

where v_i are the components of the particle velocity vector in the medium, λ and μ are the Lamé parameters, σ_{ij} are the components of the stress tensor, and f_i are the components of the external force per unit volume.

As noted above, the scattering of ultrasound pulses by a stone was studied using an axisymmetric approximation in a two-dimensional geometry. A cylinder-shaped stone with an incident plane acoustic wave propagating along its axis was considered. The medium surrounding the stone was represented by water (density $\rho = 1000 \text{ kg m}^{-3}$; Lamé parameters $\mu = 0$, $\lambda = 2.25 \text{ GPa}$), and U30 concrete ($\rho = 1700 \text{ kg m}^{-3}$; $\mu = 3.83 \text{ GPa}$, $\lambda = 7.25 \text{ GPa}$) was used as the stone material [9]. The probing ultrasound pulse was a quasi-harmonic signal that had a Gaussian envelope with a central frequency of 5 MHz.

The numerical model that we developed allowed us to study the scattering process, and to construct the corresponding ultrasound image; it may therefore be considered a virtual ultrasound scanner. The acoustic waves scattered by the stone and propagating in the opposite direction in this scanner were recorded by a multielement periodic array of receivers positioned in a line perpendicular to the axis of symmetry and passing through it (Fig. 1). In the figure, the receiving array is denoted by the dotted line to the left. The parameters of the receivers were selected to be similar to those in a Philips/ATL HDI L7-4 ultrasound transducer (width $w = 0.25 \text{ mm}$; clearance between receivers $g = 0.05 \text{ mm}$; total number of receivers $M = 128$) [10]. The boundary of the area of calculation contained a perfectly matched layer (PML, see Fig. 1) in order to avoid parasitic reverberation caused by reflections from the boundaries.

Simulation of the equations of system (1)–(2) that included the above simplifications was performed using the staggered-grid finite-difference approach [11]. To approximate the derivatives, we used a centered template that considered the structure of the equations and resulted in the need to specify certain

physical values on grids that were staggered along the corresponding coordinates. Let us clarify the above using the equation for the component of stress tensor σ_{rz} as an example. We assume that coordinates (z, r, t) are specified discretely with increments (h_z, h_r, h_t) and indices (i, j, k) . The centered time derivative between the layers with indices k and $k + 1$ determines the value in the layer with index $k + 1/2$, where the values on the right side of the equation must be specified. The derivatives with respect to r and z are matched in a similar manner. As a result, equation $\frac{\partial \sigma_{rz}}{\partial t} = \mu \left(\frac{\partial v_r}{\partial z} + \frac{\partial v_z}{\partial r} \right)$ becomes the finite-difference expression

$$\frac{\sigma_{rz_{i,j}}^{k+1} - \sigma_{rz_{i,j}}^k}{h_t} = \mu \left(\frac{v_{r_{i+1/2,j}}^{k+1/2} - v_{r_{i-1/2,j}}^{k+1/2}}{h_z} + \frac{v_{z_{i,j+1/2}}^{k+1/2} - v_{z_{i,j-1/2}}^{k+1/2}}{h_r} \right).$$

A similar procedure was performed for the rest of the equations in system (1)–(2).

Dynamics of a Spherical Bubble

There are several models for describing the dynamics of cavitation bubbles. In this work, we used the Nolting–Nepiras equation, which describes the oscillation of a spherical bubble with ideal gas in an incompressible fluid:

$$R\ddot{R} + \frac{3}{2}\dot{R}^2 = \frac{1}{\rho_0} \left[\left(p_0 + \frac{2\sigma}{R_0} \right) \left(\frac{R_0}{R} \right)^{3\gamma} - \frac{2\sigma}{R} - 4\frac{\nu}{R}\dot{R} - p_0 - p_{ac}(t) \right]. \quad (3)$$

Here, $R = R(t)$ and R_0 are the bubble radius and its initial value; ρ_0 is the density of the surrounding fluid; p_0 is atmospheric pressure; σ is the coefficient of surface tension; ν is the dynamic viscosity of the fluid; γ is the specific heat ratio of the gas in the bubble; and $p_{ac}(t)$ is the acoustic pressure of the ultrasound pulse, which is a combination of an incident wave and a wave scattered by a stone. In the simulation, it was assumed that the bubbles were located near the stone surface.

It is convenient to reduce Eq. (3) to a system of first order differential equations. If new variables $R_1 = R(t)$ and $R_2 = \dot{R}(t)$ are introduced, (3) is transformed into a system of two equations:

$$\begin{aligned} \frac{dR_1}{dt} &= R_2, \\ \frac{dR_2}{dt} &= -\frac{3(R_2)^2}{2R_1} + \frac{1}{\rho_0 R_1} \\ &\times \left[\left(p_0 + \frac{2\sigma}{R_0} \right) \left(\frac{R_0}{R_1} \right)^{3\gamma} - \frac{2\sigma}{R_1} - 4\frac{\nu}{R_1} R_2 - p_0 - p_{ac}(t) \right]. \end{aligned}$$

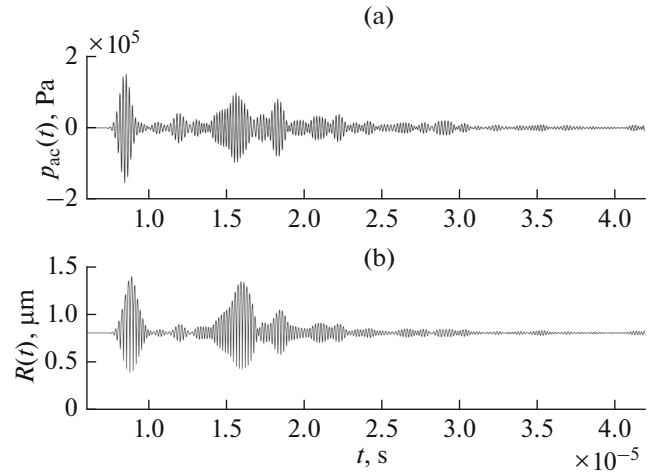


Fig. 2. (a) Pressure in the region of a bubble; (b) time dependence of the radius of the bubble.

The boundary conditions are $R_1(0) = R_0$ and $R_2(0) = 0$. In the calculations, it was assumed that the initial radius of a bubble in the absence of ultrasound was $R_0 = 0.8 \mu\text{m}$. The solution to the system was numerically calculated using the Runge–Kutta fourth-order approach [12]. To increase accuracy, we used an adaptive stepsize technique based on changing the discretization step, depending on the rate of change in the calculated function. The result from simulating the behavior of the bubble is given in Fig. 2.

Given the behavior of the radii of the bubbles over time, the acoustic field they create can be calculated. An oscillating bubble is a source of a diverging spherical wave. The potential of the particle velocity in this wave is $\varphi(r, t) = F\left(t - \frac{r}{c_0}\right)/r$, where $F(t)$ is the time function and r is the distance calculated from the bubble's center. In light of the relationship between the pressure and potential $p = -\rho_0 \partial \varphi / \partial t = -\rho_0 \dot{F}(t - r/c_0)$ and the boundary condition $\partial \varphi / \partial r|_{r=R} = \dot{R}$, we obtain the formula for the radiation of an oscillating bubble:

$$p(r, t) = \frac{\rho_0}{3r + c_0^{-1}} \frac{d^2(R^3)/d\tau^2}{dR/d\tau}, \quad (4)$$

where τ is the time of irradiation, which is associated with the current moment in time by the relation $t = \tau + [r - R(\tau)]/c_0$.

The signals arriving at the receiving array from the bubbles on the stone's surface were calculated using (4). The calculated amplitudes of the waves from the bubbles reached approximately 1 kPa. This indicated they were not too small when compared to the pressure in the probing pulse (approximately 0.2 MPa), and fell

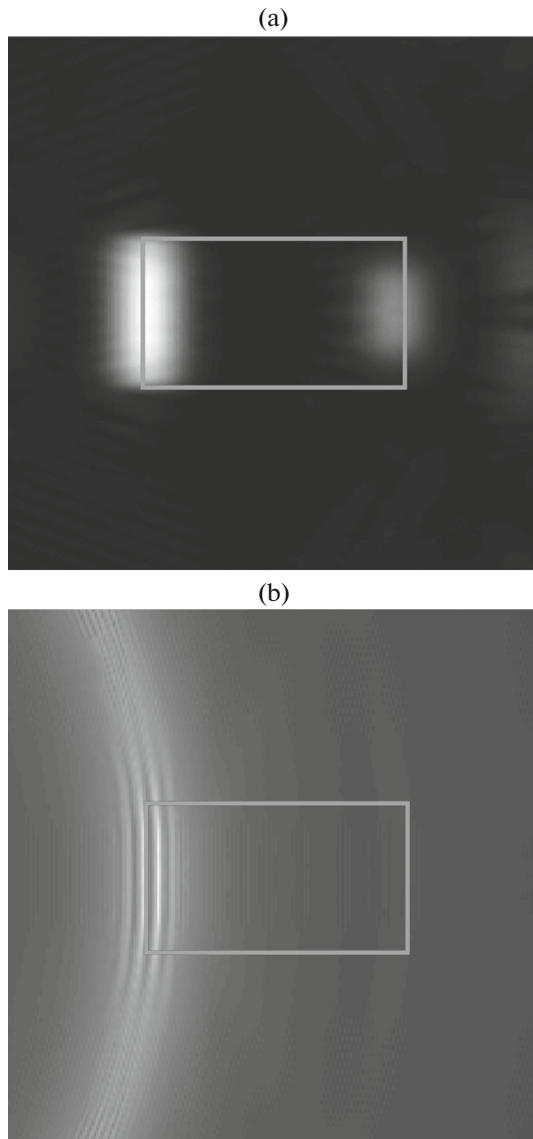


Fig. 3. (a) Image of the stone in a B-mode; (b) Doppler image after processing of the pulse ensemble.

into the dynamic range of the receiving array; i.e., it affected the scattered signal that was recorded.

SIMULATION RESULTS

As noted above, a radiation event in a Doppler mode requires the use of an ensemble of periodic pulses. In this work, we used an ensemble of 12 pulses. The repetition frequency of the pulses was selected by assuming that the incident and reflected signals did not overlap. According to [4], the bubble activity on the surfaces of kidney stones is stochastic. To satisfy this condition in the model, calculated additives to the signal from the bubbles were used for only several pulses in the ensemble.

As in real diagnostic systems, the virtual scanner had at the output of the receiving antenna array a set of 128 signals after the numerical simulation (in agreement with the number of the receiving channels). These signals were subsequently used to reconstruct the ultrasound image. Prior to image reconstruction, the signals were subjected to wall filtering [13]. This filtration suppressed the contribution from slowly moving scatterers, which can be represented by, e.g., the walls of blood vessels.

Let us briefly describe the algorithm for the Doppler processing of scattering signals. For each transducer, we consider discrete signal $W_{nm} = W_n(t_m = mh_t)$, where n is the pulse number in the Doppler ensemble, $n = 1, 2, \dots, 12$; m is the number of the time count; and h_t is the time discretization step. Analytical signal $V_{nm} = W_{nm} + iQ_{nm}$ is then constructed, where Q_{nm} is the quadrature additive of signal W_{nm} . Using the least-squares method (LSM) for an ensemble of 12 pulses, the filtered signal is calculated in the form $\bar{V}_{nm} = V_{nm} - \bar{V}_{nm}$, where $\bar{V}_{nm} = a_m + b_m n$ is the part of the signal that corresponds to slowly moving scatterers and a_m and b_m are coefficients calculated using the LSM. The power Doppler amplitude, determined as the ensemble average of the square of amplitude $U_m = \frac{1}{12} \sum_{n=1}^{12} |\bar{V}_{nm}|^2$, is then constructed for each moment in time. This procedure is performed for each of the 128 receiving elements and for each time $t_m = mh_t$, producing a final Doppler signal that can be used to reconstruct the image. For image reconstruction, we used a standard algorithm based on the summation of analytic signals with allowance for the time delays corresponding to the points of the imaged region (the delay-and-sum method) [14].

The results we obtained in the numerical experiment are given in Fig. 3. Figure 3a shows a standard brightness mode (B-mode) image, constructed using the first pulse in the Doppler ensemble. Because there were no sources of parasitic signals or other artefacts of ultrasound diagnostics in the model, the anterior and posterior borders of the kidney stone can be clearly seen in the figure, allowing us to determine its location. Figure 3b presents the result from the Doppler processing of the signal. By considering the obtained information on the stone's location, we were able to estimate the emergence of the signal near its leading edge, where the bubbles were. Since there were no other reasons for the occurrence of the signal in the experimental model, we may conclude it was bubble cavitation that caused the Doppler signal.

CONCLUSIONS

A numerical model allowed us to prove theoretically that the twinkling artefact of ultrasound diagnostics can be explained by the cavitation mechanism.

The activity of submicron bubbles on the rough surfaces of kidney stones was constructed. Quantitative analysis of the signals emitted by the bubbles during the irradiation of stones by diagnostic pulses of existing scanners showed that the waves from submicron bubbles can make a significant contribution to a scattered signal.

ACKNOWLEDGMENTS

This work was supported by the Russian Foundation for Basic Research, project no. 17-02-00261; by an RF Presidential Grant for the Leading Scientific Schools of Russia, project no. NSh-7062.2016.2; and by a personal grant from the Global Internship Program of the Focused Ultrasound Foundation (FUSF).

REFERENCES

1. Dogra, V. and Rubens, D.J., *Ultrasound Secrets*, Elsevier, 2004.
2. Rahmouni, A., Bargoin, R., Herment, A., et al., *Radiology*, 1996, vol. 199, p. 269.
3. Vasil'ev, A.Yu. and Gromov, A.I., *Voen.-Med. Zh.*, 1997, vol. 318, no. 4, p. 33.
4. Lu, W., Sapozhnikov, O.A., Bailey, M.R., et al., *Ultrasound Med. Biol.*, 2013, vol. 39, no. 6, p. 1026.
5. Kamaya, A., Tuthill, T., and Rubin, J.M., *AJR, Am. J. Roentgenol.*, 2003, vol. 180, p. 215.
6. *Moshchnye ul'trazvukovye polya* (Intense Ultrasonic Fields), Rozenberg, L.D., Ed., Moscow: Nauka, 1968.
7. Sapozhnikov, O.A., Maxwell, A.D., MacConaghy, B., and Bailey, M.R., *J. Acoust. Soc. Am.*, 2007, vol. 112, no. 2, p. 1190.
8. Mase, G.E., *Theory and Problems of Continuum Mechanics*, McGraw-Hill, 1970.
9. Cleveland, R.O. and Sapozhnikov, O.A., *J. Acoust. Soc. Am.*, 2005, vol. 118, no. 4, p. 2667.
10. Sapozhnikov, O.A. and Bailey, M.R., *J. Acoust. Soc. Am.*, 2013, vol. 133, no. 2, p. 661.
11. Vireux, J., *Geophysics*, 1986, vol. 51, p. 889.
12. Kalitkin, N.N., *Chislennyye metody* (Numerical Methods), Moscow: Nauka, 1978.
13. Thomas, L. and Hall, A., in *Proc. IEEE Ultrasonics Symp.*, Cannes, 1994, vol. 3, p. 1701.
14. Synnevag, J.F., Austeng, A., and Holm, S., *IEEE Trans. Ultrason., Ferroelectr., Freq. Control*, 2007, vol. 54, no. 8, p. 1606.

Translated by E. Berezhnaya